On the role of built-in electric fields on the ignition of oxide coated nanoaluminum: Ion mobility versus Fickian diffusion

Brian J. Henz,[1] Takumi Hawa,[2] and Michael R. Zachariah[2,a)]
[1]*U.S. Army Research Laboratory, Aberdeen Proving Ground, Maryland, 21005, USA*
[2]*Department of Mechanical Engineering and the Department of Chemistry and Biochemistry, University of Maryland, College Park, Maryland, 20742, USA*

(Received 26 May 2009; accepted 16 August 2009; published online 19 January 2010)

Using the classical molecular dynamics method we simulate the mechanochemical behavior of small (i.e., core diameter < 10 nm) oxide coated aluminum nanoparticles. Aluminum nanoparticles with core diameters of approximately 5 and 8 nm are simulated with 1 and 2 nm thick oxide coatings or shells. In addition to thickness the shells are parametrized by varying degrees of crystallinity, density, and atomic ratios in order to study their effect on the ignition of nanoparticle oxidation. The oxide shells are parametrized to consider oxide coatings with the defects that commonly occur during the formation of an oxide layer and for comparison with a defect free crystalline oxide shell. Computed results include the diffusion coefficients of aluminum cations for each shell configuration and over a range of temperatures. The observed results are discussed and compared with the ignition mechanisms reported in the literature. From this effort we have found that the oxidation ignition mechanism for nanometer sized oxide coated aluminum particles is the result of an enhanced transport due to a built-in electric field induced by the oxide shell. This is in contrast to the currently assumed pressure driven diffusion process. This induced electric field accounts for approximately 90% of the mass flux of aluminum ions through the oxide shell. The computed electric fields show good agreement with published theoretical and experimental results. © *2010 American Institute of Physics*. [doi:10.1063/1.3247579]

I. INTRODUCTION

Much of the interest in nanoparticles is derived from an appreciation that chemical/physical properties often vary from that of the bulk material. Some of these properties, including increased reactivity,[1] can simply be attributed to the high surface area to volume ratio of nanoparticles; however, it is known that catalytic activity can be significantly changed from that of the corresponding bulk.[2,3] It is also well known that metal nanoparticles are pyrophoric and have enhanced energy release rates, which make them attractive in propulsion.[4]

Virtually all metal nanoparticles will nominally have a native oxide shell, which for aluminum is $\sim 2-3$ nm thick. Thus any oxidative reaction or vigorous combustion must proceed by transport of either the aluminum or oxidizer though the oxide shell. The ignition temperature of oxide coated aluminum nanoparticles has been observed to decrease with particle size, with a minimum temperature reached for nanoparticles near the melting point of the aluminum core.[5] This suggests to some that a mechanism associated with the melting of the aluminum core is responsible for ignition, whereas in larger particles the ignition temperature is closer to the melting temperature of alumina, namely, 2327 K. The closeness of the reaction temperature to the melting point of pure aluminum indicates that the melting of the aluminum core is the possible initiator of this reaction for nanoparticles.

It has previously been assumed that either the sudden decrease in density of the aluminum upon melting[6,7] or the lower melting temperature of the nanometer sized oxide shell[8] is the key to initiation of the oxidation process. However, in this paper we explore the possibility that built-in electric fields as opposed to Fickian diffusion drive aluminum cations through the oxide shell to the nanoparticle surface where it is possible for the oxidation process to proceed. Experimentally produced hollow aluminum oxide nanoparticles provide support for this rapid diffusion hypothesis.[9,10] These observed hollow oxide shells are an indication that the oxidation process is driven by the diffusion of aluminum cations. We will show that field mediated ion-transport is much faster than Fickian diffusion and will be the dominant transport process in the initiation of the oxidation of nanoaluminum. Anecdotal support for this mechanism comes from numerous numerical[11,12] and experimental studies.[13,14]

II. SIMULATION APPROACH

In this work we have chosen to use the ReaxFF (reactive force field) empirical potential from van Duin[15] implemented within the GRASP (general reactive atomistic simulation program) molecular dynamics (MD) application. The ReaxFF potential has an advantage over traditional empirical potentials in that it is able to accurately simulate the charge transfer that occurs during metal oxidation. The other empirical potential commonly used for this material system is the Streitz–Mintmire potential;[16] however, we chose to use the ReaxFF potential because it is available within GRASP, which can be executed in parallel. The Al–O potential pa-

a)Author to whom correspondence should be addressed. Electronic mail: mrz@umd.edu.

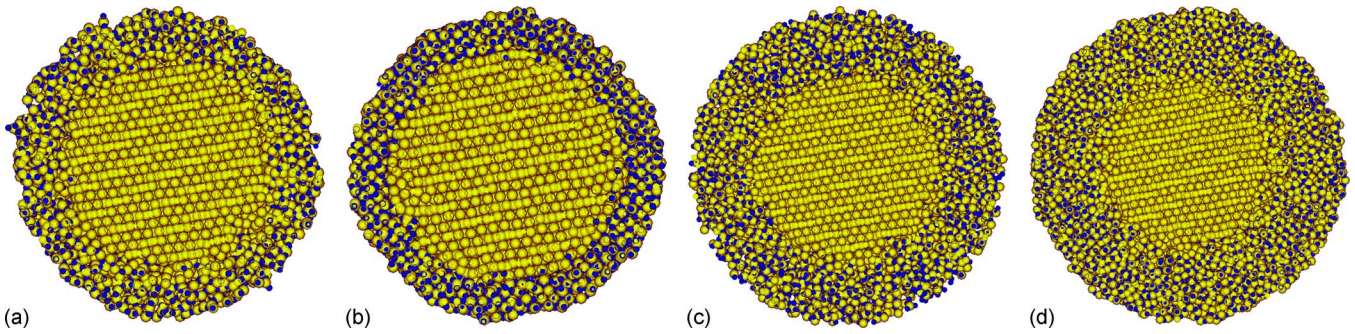

FIG. 1. (Color online) Cross sections of some of the oxide coated aluminum nanoparticle models used in this work. (a) 1 nm thick, dense oxide shell. (b) 1 nm thick, crystalline oxide shell. (c) 2 nm thick, amorphous oxide shell. (d) 2 nm thick, dense oxide shell with 2:2.7 Al:O ratio. Blue (dark) spheres represent oxygen atoms and yellow (light) spheres denote aluminum atoms.

rameter set used in this work comes from a previous effort that considered the sliding of Al_2O_3 coatings against Al and Al_2O_3.[17] The computational requirement of this software is high with the largest material system considered here containing nearly 100 000 atoms and requires 96 Intel Woodcrest processor cores running at 3.0 GHz to be simulated efficiently.

III. MODEL DESCRIPTION

Two core sizes are considered here, the smaller of these consists of a 5.6 nm diameter core of aluminum with either a 1 or 2 nm thick shell of alumina (Al_2O_3) as illustrated by the example systems in Fig. 1. The larger model includes an 8 nm aluminum core with a 2 nm thick crystalline oxide shell (Fig. 2). This model is used to consider scaling effects for the electric field and diffusivity.

There are four shell configurations considered for each oxide shell thickness.

(1) A defect free crystalline shell that may result from extremely slow or high temperature formation. This shell is modeled by coating a bare aluminum nanoparticle with a crystalline shell made up of α-Al_2O_3. Although the gamma phase of alumina is more prevalent in oxide coated nanoparticles the alpha form is also observed and is a limiting case as it is the densest phase that the oxide shell will form. A dense amorphous shell has an atomic ratio of 2:3 aluminum to oxygen atoms (i.e., Al_2O_3). This shell is formed in the simulation by heating a crystalline oxide shell above its melting temperature while holding the aluminum core atom positions fixed. In this way the oxide layer melts and then is rapidly cooled and trimmed in order to obtain a slightly amorphous oxide layer with the desired thickness.
(2) A dense amorphous shell 10% deficient in oxygen atoms, Al/O=2:2.7. This shell may form during a faster rate of formation or if the environment during formation was oxygen lean. In the computer simulation this shell is formed by removing 10% of the oxygen from the previous dense oxide shell that is at the stoichiometric ratio of 2:3 aluminum to oxygen atoms.
(3) Lastly, a porous amorphous shell with an atomic ratio of 2:3 aluminum to oxygen atoms. This shell has approximately one-half of the density of the previously described dense shell with the same atomic ratio. This more porous amorphous shell represents oxide formation that may occur at a very fast rate with a sufficient supply of oxygen. This oxide shell is formed in the computer simulation similarly to the process used for the dense shell except that the shell is repeatedly heated to a higher temperature and rapidly cooled until a much more amorphous configuration is achieved.

Following the creation and equilibration of the oxide shell, the model systems were heated at rates of 10^{11}, 10^{12}, and 10^{13} K/s in order to determine any rate dependencies. We found, similarly to Puri and Yang,[8] that at rates below 10^{12} K/s the heating rate appears to have little effect on the simulation results. This is an important result, as lower heating rates would increase the number of MD simulation time steps, which for this work was ~1 fs to maintain energy conservation, to a level that would be unreasonable with current computing capacities. The temperature of the model systems was raised from 300 to 1000 K and eventually up to 3000 K, which is much higher than the melting point of the oxide layer. From experimental data available in the literature[4] it is expected that some reaction should be observed near the melting point of the aluminum core. At the melting point of the core the aluminum density decreases from 2.7 to 2.4 g/cm^3, resulting in a volumetric expansion of about 12%. Melting of the oxide shell requires heating the nanoparticle to above the melting point of the oxide which is 2327 K for the bulk material or somewhat less for a nanoparticle shell because of the size affect. The results of each of these efforts are detailed in the following sections.

IV. RESULTS OF RAPID HEATING SIMULATIONS

The simulations in this section were carried out in a vacuum so that as Al cations move radially outward toward the oxide surface there are no oxygen molecules available for oxidation reactions. In simulations discussed later we have found the diffusivity of Al through the oxide layer to be more important than oxygen diffusion toward the core. For this reason we are primarily concerned in this work with the mechanism by which Al cations reach the surface of the nanoparticle, therefore limiting the scope of this effort to the ignition process. Initially, the nanoparticles were heated from 300 to about 1000 K, which is above the core melting point

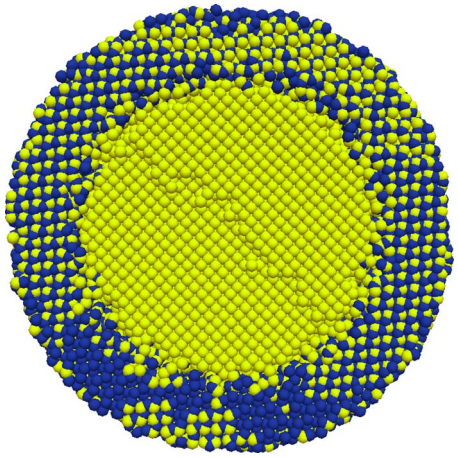

FIG. 2. (Color online) Cross section of an 8.2 nm Al core with 2 nm thick crystalline oxide shell. Yellow (light) denotes Al atoms and oxygen atoms are blue (dark).

but below the size dependent oxide melting point reported by Puri and Yang.[8] At around 900 K, or slightly below the bulk melting temperature of the aluminum core, a rapid volumetric expansion of the core is observed indicating that the aluminum core has begun to melt. At 1000 K the oxide shell still remains intact, with no cracking, even when maintained at that temperature for 100 ps. We do see, however, as illustrated in Fig. 2, the initiation of aluminum cation diffusion to the particle surface.

The results in Fig. 2 show a slightly inhomogeneous melting of the aluminum core, which is evident in the "1000 K, +0 ps" plot. Some of the less dense faces of the core begin to melt while the top and bottom remain crystalline, giving the nanoparticle a slightly elongated appearance. The plots in Fig. 2 also demonstrate the mechanism by which oxidation will be initiated at elevated temperatures. The first observation is that the oxide shell does not crack as one might expect if diffusion were extremely limited, or the shell were brittle. This suggests that the shell is more elastic at this length scale, or the expansion of the aluminum is insufficient to cause failure in the shell, even at these elevated temperatures. One possible reason for the enhanced elasticity is the lower coordination of the atoms in the oxide shell as compared to the bulk material,[18] which is incidentally also a contributing factor to the size dependent melting temperature observed in nanoparticles. In addition, we observe significant diffusion of the core atoms through the oxide shell, thus relieving the potentially high internal pressures. The primary mechanism driving this diffusion is discussed in the following sections.

V. ALUMINUM CATION DIFFUSION THROUGH THE OXIDE SHELL

As observed by us and by others,[8] at temperatures below the melting point of the oxide shell there is significant diffusion of aluminum cations through the oxide shell. Computation of the diffusivity from the mean square displacement (MSD) of the aluminum cations yields values typically found for liquids. This was unexpected because these measurements were taken at 600 K, somewhat below the melting temperature of the relatively small 5.6 nm aluminum nanoparticle core. Although the MSD data are somewhat noisy because of the limited simulation time and small nanoparticle sizes, there is an obvious trend of proportionally increasing diffusion rates radially through the shell with increased temperature. To support this observation the radial diffusivity is compared to the overall diffusivity in Table I.

The diffusion coefficients in Table I are computed using Eq. (1),

$$\frac{\partial\langle r^2(t)\rangle}{\partial t} = 2dD. \tag{1}$$

In Eq. (1), the number of dimensions, d, available for atomic diffusion, is 3 for overall diffusion, and 1 for radial diffusion.[19] The use of the bulk diffusion equation is reasonable since during the time scales considered the movement of only the atoms initially on the surface are restricted by the particle boundary.[20] For radial diffusion we are only concerned with the MSD directed radially from the center of the nanoparticle. In Eq. (1), t is the elapsed time and $\langle r^2(t)\rangle$ is the MSD of the atoms being tracked. The diffusion coefficients reported are for all of the core atoms including those near the center of the nanoparticle. This is important since we would expect the mechanical and electrostatic effects to be larger near the core/shell interface, but because of the small sample sizes available, computing a radial distribution of diffusivity is unreliable.

By comparing the radial and overall diffusivities in Table I an interesting trend is observed. As the temperature increases the radial diffusivity becomes a generally more important portion of the overall diffusivity of aluminum cations. This result indicates that once the aluminum core has melted the diffusion of aluminum cations is preferentially in the radial direction, as compared to the results prior to melting. This is possibly due to a high pressure gradient near the core/shell interface pushing atoms out into the shell. Another possibility is that once the core has melted the atoms are more mobile so in addition to pressure, any other effects such as an electric field will increase diffusion. The radial diffusion data that do not correlate with this observation at 600 K are for the 2 nm thick crystalline oxide shells for both the 5.6 and 8.2 nm aluminum cores. These configurations show diffusion rates that are on par with the overall diffusivity, possibly indicating that one of the drivers of radial diffusion is proportionally stronger for these shell configurations at 600 K. We will show in the following sections that the electric field is indeed strongest in the 2 nm thick crystalline shells.

In Fig. 3 an Arrhenius plot of the diffusivity versus temperature is given for each of the oxide shell configurations used with the 5.6 nm aluminum core in this work. From Fig. 3 we observe that a change in slope occurs near the melting point of the aluminum core, namely, 1000 K. This indicates that for temperatures above 1000 K the activation energy required for cation diffusion is lower than for temperatures below 1000 K. The increase in activation energy for the 1 nm amorphous and dense oxygen poor shells is likely due to a lower melting point for these oxide shells. This is not the case for thicker or more crystalline shells where the oxide

TABLE I. Effective diffusion coefficients for core aluminum atoms with various oxide shell configurations. The effective diffusion coefficients are for general diffusion (D_{eff}) and radial diffusion (D_{radial}).

Shell thickness	Type	Temperature	D_{eff} (cm^2/s^*10^{-7})	D_{radial} (cm^2/s^*10^{-7})
1 nm	Amorphous	600 K	53	5.9
1 nm	Amorphous	1000 K	420	300
1 nm	Amorphous	2000 K	7100	8300
1 nm	Dense	600 K	11	4.0
1 nm	Dense	1000 K	340	280
1 nm	Dense	2000 K	1300	1300
1 nm	Dense, $Al_2O_{2.7}$	600 K	2.6	2.1
1 nm	Dense, $Al_2O_{2.7}$	1000 K	380	190
1 nm	Dense, $Al_2O_{2.7}$	2000 K	6000	6700
1 nm	Crystalline	600 K	31	6.7
1 nm	Crystalline	1000 K	330	240
1 nm	Crystalline	2000 K	1000	1300
2 nm	Amorphous	600 K	23	4.6
2 nm	Amorphous	1000 K	400	320
2 nm	Amorphous	2000 K	770	660
2 nm	Dense	600 K	8.1	6.9
2 nm	Dense	1000 K	360	250
2 nm	Dense	2000 K	490	520
2 nm	Dense, $Al_2O_{2.7}$	600 K	4.2	3.3
2 nm	Dense, $Al_2O_{2.7}$	1000 K	370	180
2 nm	Dense, $Al_2O_{2.7}$	2000 K	270	100
2 nm	Crystalline	600 K	8.3	7.8
2 nm	Crystalline	1000 K	330	190
2 nm	Crystalline	2000 K	490	520
2 nm, 8 nm core	Crystalline	600 K	6.9	9.9
2 nm, 8 nm core	Crystalline	1000 K	190	160
2 nm, 8 nm core	Crystalline	2000 K	1300	920

remains in the solid phase and does not undergo any phase transformation. In the remaining model systems the activation energy drops once the melting temperature is reached, indicating a change in diffusion mechanism. The primary change that occurs at around 1000 K is the melting of the aluminum core, the associated volumetric expansion, and increased mobility of the aluminum atoms. This expansion is expected to greatly increase the pressure inside of the core, and enhance the diffusion of aluminum cations radially outward through the oxide shell (Fig. 4).

VI. INDUCED ELECTRIC FIELD IN OXIDE SHELL

One possible explanation for the computed rapid diffusion of aluminum atoms through the oxide layer is that they are driven by an induced electric field near the core/shell interface. The theory that oxidation growth proceeds via migration of charged particles is not a new one. In fact Carl Wagner proposed this theory in 1933.[13] In a 1948 paper by Cabrera and Mott[11] the authors developed a theory focused on the growth of a thin oxide film on metal surfaces that is driven by an induced electric field. This electric field causes metal ions to migrate to the surface, increasing the oxide thickness until the induced field is prevented by the thickening surface to cause further diffusion of metal cations. The maximum thickness of the oxide layer that is formed with this process increases with temperature, up to a critical temperature above which growth of the oxide layer will continue indefinitely.

Recent theoretical and experimental evidence points to the importance of the induced electric field described by Cabrera and Mott in the oxidation of oxide coated metal nanoparticles. Zhdanov and Kasemo[21] recently performed an analysis of the induced electric field in oxide coated nanoparticles. They found that by considering the size and geometry effect of nanoparticles coated with oxide shells that the induced electric field will be much stronger than observed in a flat surface, thus increasing the associated oxidation rate exponentially in oxide coated nanoparticles. We have also observed the formation of hollow particles [Ref. 9, Fig. 2.] during the oxidation of oxide coated aluminum, which we attributed to the faster diffusion of Al cations. Subsequently Nakamura *et al.*[10] also observed formation of hollow metal oxide nanoparticles from oxidation of metals and attributed the rapid diffusion of metal cations through the oxide shell to the induced electric field. In the following sections we investigate the magnitude and effect of the induced electric field on the oxide coated aluminum nanoparticle system.

In the current simulation effort, rapid diffusion of aluminum cations through the oxide layer is observed. An indicator of the strength of the electric field is the radial charge density. The radial charge density is computed through the nanoparticle at 2 Å radial intervals and is averaged over 100

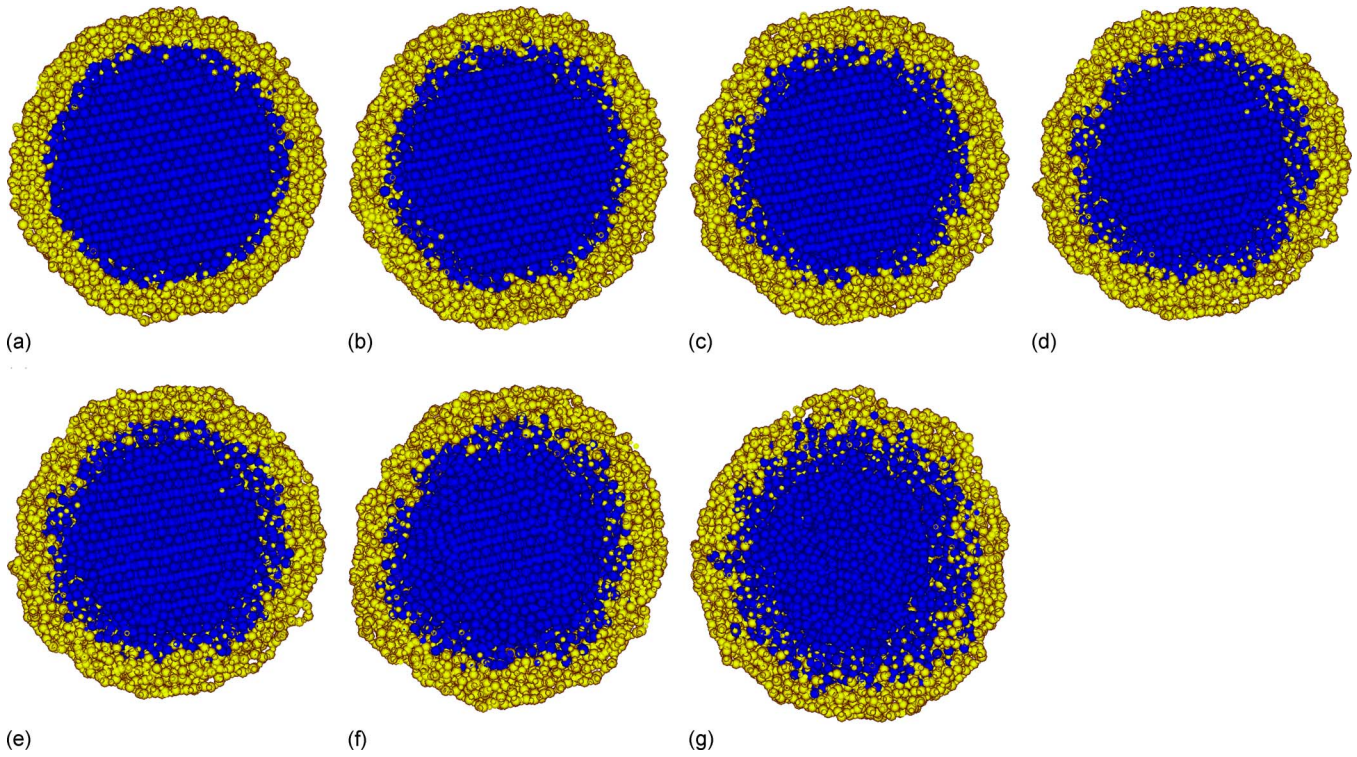

FIG. 3. (Color online) Plot showing diffusion of aluminum cations (blue, dark) through the 1 nm thick oxide shell (yellow, light) as the temperature increases from 300 to 1000 K and held for 100 ps.

ps of simulation time, Fig. 5. Although noisy, which is partially caused by atomic diffusion, it is apparent that there is a negative charge gradient throughout the oxide shell. This charge gradient contributes to the out flow of positive charges, and the mass flux of aluminum cations at the core/shell interface.

The difference in charge density between the inner and outer surfaces of the oxide shell indicates that an electric field is induced, which will drive aluminum cations near the core/shell interface to the outer surface where they will be exposed to oxygen and oxidize. An approximate interaction between an aluminum cation, with the core and shell can be computed using Gauss's Law. By assuming the atomic charges to be distributed approximately homogeneously in the shell and the core, the electric field on the surface of the core can be estimated as the field from a single point charge at the center of the core, through Eq. (2). If we assume the charge to be evenly distributed in the oxide shell then the electric field inside of the shell from the atoms in the oxide shell is zero,

$$E = \frac{Q_{\text{core}}}{4\pi\varepsilon_0 r^2}. \tag{2}$$

In Eq. (2), Q_{core} is the total charge of the core, r is the radial position of the interfacial aluminum atom of interest, and ε_0 is the permittivity of a vacuum. Using Eq. (2) the electric

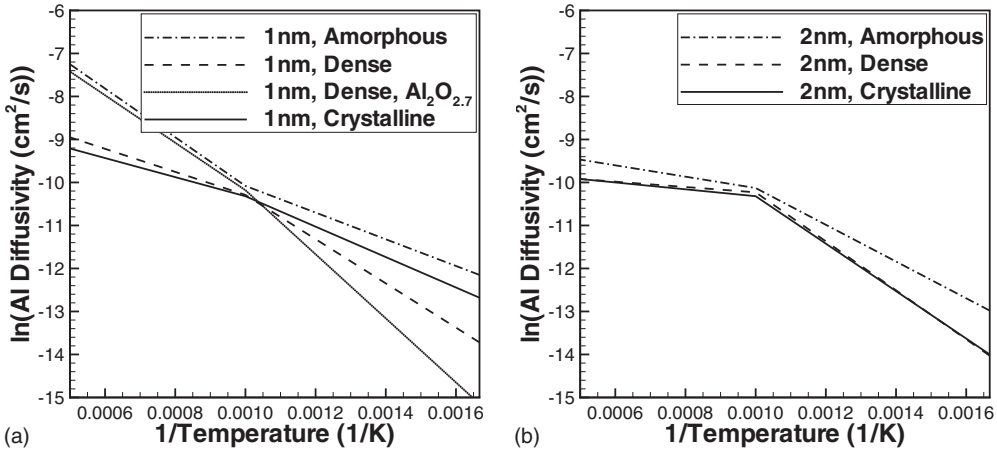

FIG. 4. Arrhenius plot of $\ln(d)$ vs $1/T$, where D is the diffusivity of the core aluminum atoms. The slope of this plot is the activation energy required for diffusion of aluminum cations and shows an expected decrease above the melting point of the core, at approximately 0.001/K.

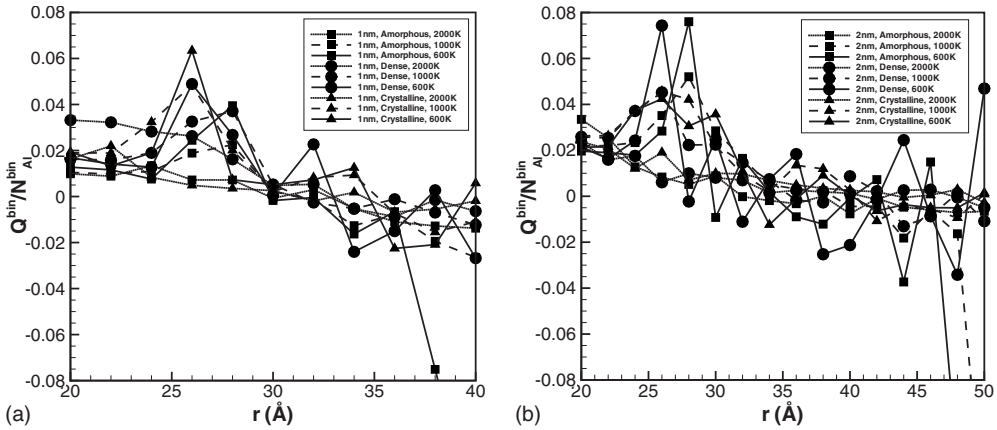

FIG. 5. Radial charge distribution through the oxide shell for a 1 nm (a) thick shell and a 2 nm (b) thick shell.

fields from the various oxide coated models are computed in Table II.

In Fig. 6 the volume between the core surface and outer surface of the oxide shell is assumed to be a vacuum. For the purpose of computing the electric field, this assumption is valid so long as the charges in the oxide shell are distributed radially only. With a radially distributed charge the electric field due to the oxide shell is zero everywhere for atoms at the core/shell interface or inside of the aluminum core. The most obvious trend observed in Table II is that of the decreasing core charge and electric field strength with increasing temperature. This is likely due to the fact that as shown in Table I, diffusivity increases as temperature increases, and smears the boundary between the core and shell. Another observed trend, albeit weaker, is an increase in the electric field as the shell becomes thicker, and more organized. So in going from an amorphous 1 nm thick shell to a 2 nm thick crystalline shell we observe a 100% increase in the electric field strength. This observation is supported by the analysis of Zhdanov and Kasemo.[21]

TABLE II. Total charge of aluminum core and associated electric field are given here for all of the core/shell configurations considered. Note on electric field units, $N/C=0.01$ V/m.

Shell thickness	Type	Temperature	Q_{core} (C^*10^{-18})	E (N/C^*10^{10})
1 nm	Amorphous	600 K	8.28	1.10
1 nm	Amorphous	1000 K	5.67	0.75
1 nm	Amorphous	2000 K	1.47	0.20
1 nm	Dense	600 K	11.4	1.52
1 nm	Dense	1000 K	8.86	1.18
1 nm	Dense	2000 K	4.01	0.53
1 nm	Dense, $Al_2O_{2.7}$	600 K	7.91	1.05
1 nm	Dense, $Al_2O_{2.7}$	1000 K	6.38	0.85
1 nm	Dense, $Al_2O_{2.7}$	2000 K	1.09	0.14
1 nm	Crystalline	600 K	12.7	1.69
1 nm	Crystalline	1000 K	10.8	1.44
1 nm	Crystalline	2000 K	3.04	0.40
2 nm	Amorphous	600 K	13.3	1.77
2 nm	Amorphous	1000 K	11.9	1.58
2 nm	Amorphous	2000 K	4.61	0.61
2 nm	Dense	600 K	13.8	1.83
2 nm	Dense	1000 K	12.7	1.69
2 nm	Dense	2000 K	4.21	0.56
2 nm	Dense, $Al_2O_{2.7}$	600 K	11.6	1.54
2 nm	Dense, $Al_2O_{2.7}$	1000 K	11.1	1.47
2 nm	Dense, $Al_2O_{2.7}$	2000 K	7.80	1.04
2 nm	Crystalline	600 K	15.6	2.08
2 nm	Crystalline	1000 K	13.9	1.85
2 nm	Crystalline	2000 K	4.39	0.58
2 nm, 8 nm core	Crystalline	600 K	43.9	2.47
2 nm, 8 nm core	Crystalline	1000 K	42.6	2.40
2 nm, 8 nm core	Crystalline	2000 K	30.4	1.71

A more accurate method of computing the electric field at each ion in the core and shell is to use Coulomb's Law and to sum the discrete contribution from all of the neighboring charges. Using this method is straight forward since there are finite numbers of discrete charge carrying atoms. In Fig. 7 the computed electric field, using Eq. (3), is plotted at each of the core aluminum atoms,

$$E = \frac{q}{4\pi\varepsilon_0 r^2}\hat{e}_r. \tag{3}$$

In Eq. (3) $\hat{e}_r$ is the radial unit vector coming from the neighboring atom and q is the charge associated with the neighboring atom. Summing each of these vectors for all of the core atoms gives the results as shown in Fig. 7 for 600, 1000, and 2000 K.

The electric field plotted in Fig. 7 is within one order of magnitude of the simple model results, tabulated in Table II, which assumes a homogeneous charge distribution in the core and oxide shell. The direction of the computed electric field indicates that the mass flux due to the electric field is directed out through the oxide shell rather than acting to randomly rearrange the atoms. The positively charged alumi-

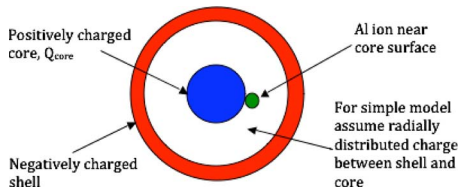

FIG. 6. (Color online) Schematic of assumed charge distributions affecting electric field around core surface aluminum atoms.

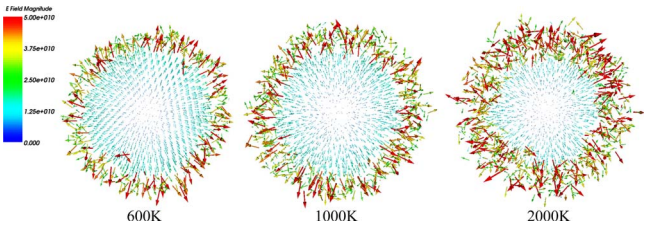

FIG. 7. (Color online) Electric field (N/C) at each of the core Al atoms in the nanoparticle core computed using Coulomb's Law. These results are for the 5.6 nm core with a 2 nm thick crystalline shell. Note the generally radial direction of the field.

num atoms will therefore be preferentially directed toward the outer surface of the oxide shell, where they will come into contact with oxygen ions and oxidize.

With the diffusion coefficients previously computed and the electric field results computed here it is possible to analyze the mass flux due to concentration gradients (J_d), the electric field (J_e), and the internal pressure (J_c). The relative magnitude of the effect of the electric field on Al ion diffusion can be computed using the Nernst–Planck equation. The Nernst–Plank equation is given in Eq. (4),[22]

$$J = -D\frac{dC}{dx} - \frac{zFDC}{RT}\frac{d\phi}{dx} + Cv, \tag{4a}$$

$$J = J_d + J_e + J_c. \tag{4b}$$

If we assume a zero molar concentration of Al cations in the shell and the bulk concentration at the interface then the parameters for Eq. (4a) are given as the following:

$$C = 0.1 \ \text{mol/cm}^3,$$

$$\frac{dC_{1\ \text{nm}}}{dx} = 1.0 \times 10^6 \ \text{mol/cm}^4,$$

$$R = 8.314 \ \text{C V/mol K},$$

$$F = 96485 \ \text{C/mol}. \tag{5}$$

The electric field computed in Table II is the negative of the charge gradient $d\varphi/dx$.

The convective flux, J_c in Eq. (4) is the drift velocity of metal ions through the core/shell interface due to constant force acting on the ions. The force on these ions comes from the pressure gradient, which is due to the expanding aluminum melt. When considering J_c only the radial drift velocity, and therefore the radial pressure gradient, in Eq. (4a) is considered so that J_c can be rewritten as $C\,(Df_r/k_BT)$, where f_r is defined as

$$f_r = -\frac{\partial V}{\partial r} = -\nabla p v_{\text{Al}}. \tag{6}$$

In Eq. (6), ∇p is the pressure gradient in the radial direction and v_{Al} is the solubility of Al in the Al_2O_3 network.[23] The maximum pressure gradients observed in the simulations range from less than 1 GPa/nm at 600 K to 2 GPa/nm at 1000 K and above. For the solubility of Al in Al_2O_3 we have assumed a value that comes from previous analysis of oxygen and Al diffusion through Al_2O_3 and should therefore be a reasonable value. Assuming a value of about 0.02 nm^3 for the solubility of Al, v_{Al}, it is possible to estimate the mass flux due to each term in Eq. (4). The diffusivity due to the drift velocity is directly proportional to v_{Al} but variations here by less than one order of magnitude and would have little effect on the results in Table III.

From the final column in Table III, listing the ratio of J_e to J, it is apparent that in all cases except for two, over 90% of the mass flux through the oxide shell is due to the induced electric field present at the core/shell interface. The exceptions to this 90% observation are the 1 nm amorphous and 1 nm dense $Al_2O_{2.7}$ shells at 2000 K, which from previous analysis appear to have undergone a phase change at this temperature. This illustrates the importance of considering the electric field in the oxide shell for any oxidation analysis of the oxide coated aluminum nanoparticle system. Another interesting trend is that the importance of the electric field in diffusion increases, as both the shell thickens and the temperature decreases. The trend associated with temperature is expected since diffusion without an electric field is strongly temperature and pressure dependent, and at low temperatures diffusion would be very slow without an electric field. The trend associated with shell thickness requires some more thoughtful analysis. By considering the computed electric fields in Table II, we observe that the magnitude does indeed increase with shell thickness while the overall mass flux decreases, Table II and Fig. 8.

In Fig. 8 we observe some interesting trends not necessarily apparent in Table III. For nanoparticle systems at 600 and 1000 K the degree of crystallinity in the oxide shell does not appear to have a noticeable effect on the mass flux of the aluminum cations through the oxide shell. This result is interesting because we can conclude that the reaction rate for oxide coated aluminum nanoparticles in this size range will not be dependent on how the coating was formed or upon its thickness, up to 2 nm.

The most apparent trend in Fig. 8 is that the mass flux of aluminum atoms through the shell at 2000 K decreases with increasing shell crystallinity and thickness. This result is likely due to the increased dependence of total mass flux on the concentration gradient and drift velocity terms in Eq. (4) as opposed to being solely due to the electric field. This decreased mass flux is observed as lower values in the last column in Table III for 2000 K versus 600 and 1000 K. Since the heating rate required to reach 2000 K before an appreciable amount of the core has diffused into the shell is so high, greater than 10^{12} K/s, we would not expect this to be an experimentally observable result without some sort of very rapid heating method.

VII. FORMATION OF HOLLOW ALUMINUM OXIDE SHELLS

Recent experimental efforts by Rai *et al.*[9] and Nakamura *et al.*[10] have both observed the formation of hollow aluminum oxide nanoparticles as a result of the oxidation of oxide coated aluminum nanoparticles. In the work by Rai *et al.*[9] we observed the formation of hollow spheres of aluminum oxide subsequent to the oxidation of aluminum nanoparticles at

TABLE III. Diffusion coefficient and mass flux computed at 600, 1000, and 2000 K for all shell configurations with the 5.6 nm core unless noted. The last column labeled ratio $J_e:J$, is the fraction of the total mass flux due to the induced electric field, with the balance due to the concentration gradient and drift velocities.

Shell thickness	Configuration	Temperature	J (mol/cm^2 s)	D (cm^2/s*10^{-8})	Ratio $J_e:J$
1 nm	Amorphous	600 K	4.20	1.97	0.98
1 nm	Amorphous	1000 K	11.97	13.6	0.96
1 nm	Amorphous	2000 K	53.45	424.0	0.83
1 nm	Dense	600 K	3.03	1.03	0.99
1 nm	Dense	1000 K	11.49	8.33	0.97
1 nm	Dense	2000 K	35.18	110.8	0.93
1 nm	Dense, $Al_2O_{2.7}$	600 K	2.13	1.03	0.98
1 nm	Dense, $Al_2O_{2.7}$	1000 K	8.06	7.88	0.96
1 nm	Dense, $Al_2O_{2.7}$	2000 K	46.27	426.0	0.78
1 nm	Crystalline	600 K	5.08	1.55	0.99
1 nm	Crystalline	1000 K	14.72	8.75	0.98
1 nm	Crystalline	2000 K	35.58	147.0	0.91
2 nm	Amorphous	600 K	3.31	0.97	0.99
2 nm	Amorphous	1000 K	18.49	10.0	0.98
2 nm	Amorphous	2000 K	23.73	65.2	0.94
2 nm	Dense	600 K	1.26	0.35	0.99
2 nm	Dense	1000 K	6.13	3.11	0.98
2 nm	Dense	2000 K	11.34	33.8	0.93
2 nm	Dense, $Al_2O_{2.7}$	600 K	3.69	1.23	0.99
2 nm	Dense, $Al_2O_{2.7}$	1000 K	7.99	4.58	0.98
2 nm	Dense, $Al_2O_{2.7}$	2000 K	5.27	8.38	0.96
2 nm	Crystalline	600 K	7.83	1.94	0.99
2 nm	Crystalline	1000 K	15.06	6.98	0.98
2 nm	Crystalline	2000 K	6.81	19.6	0.93
2 nm, 8 nm core	Crystalline	600 K	17.27	3.59	0.99
2 nm, 8 nm core	Crystalline	1000 K	24.31	8.61	0.99
2 nm, 8 nm core	Crystalline	2000 K	31.27	30.8	0.98

about 727 K. We expected that these hollow oxide shells are produced by the outward diffusion of aluminum through the oxide shell as opposed to inward diffusion of oxygen. This observation is supported here by the high measured diffusion coefficients for aluminum cations and mass flux due to the electric field in the nanoparticle.

In order to better compare the inward diffusion of oxygen versus the outward diffusion of aluminum we have simulated a 5.6 nm aluminum core with a 2 nm crystalline oxide shell in a high density oxygen gas as shown in Fig. 9. The diffusion of oxygen ions through the shell has the potential to

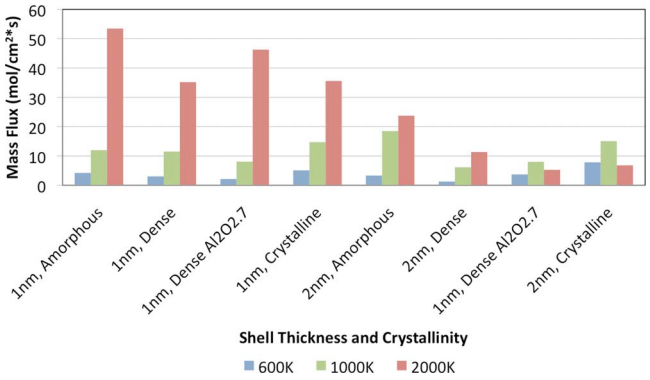

FIG. 8. (Color online) Plot of mass flux vs temperature and shell configuration.

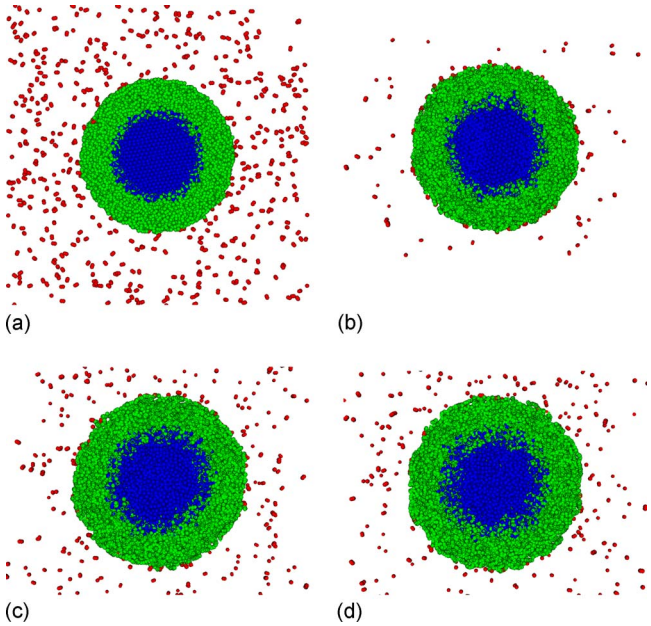

FIG. 9. (Color online) Cross section of oxide (green) coated aluminum core (blue, dark) showing surrounding oxygen (red) atoms. Higher rates of diffusion for aluminum cations is observed by aluminum atoms moving radially outward into the oxide shell atoms while adsorbed oxygen atoms remain on the outer surface or desorb from the shell. (a) and (b) are at 600 K and represent 10 and 100 ps of simulation time, respectively. (c) and (d) are at 1000 K, after 10 and 100 ps, respectively.

limit the mass flux of aluminum cations emanating from the core, producing reactions inside of the oxide shell and at the core/shell interface as opposed to on the nanoparticle surface. Oxidation in the core would potentially increase the internal pressure of the nanoparticle from volumetric expansion resulting in mechanical failure of the oxide shell, but would be unlikely to result in the hollow shells observed by Rai *et al.*[9]

In Fig. 9 it is apparent that the diffusivity of aluminum cations through the oxide shell is observably higher than the diffusion rate of oxygen anions toward the core. This result indicates that oxidation will occur on or near the outer surface of the oxide shell rather than at or near the core/shell interface. By the oxidation reaction occurring on the outer shell surface an outward growth of the oxide shell is observed which ultimately results in a hollow aluminum oxide shell as observed experimentally.[9,10] One effect that may limit the mass flux of oxygen atoms into the oxide shell is that at higher temperatures the sticking probability of the gas molecules is lower than for temperatures < 623 K.[24]

VIII. CONCLUSIONS

For small oxide coated aluminum nanoparticles we have found that ignition of the oxidation process is likely to occur by rapid diffusion of aluminum cations through the oxide shell as opposed to mechanical failure or melting of the shell, for heating rates as high as 10^{12} K/s. The high level of measured aluminum cation diffusivity is driven not only by the volumetric expansion of the aluminum core, but primarily by the induced electric field in the oxide shell. This enhanced diffusivity due to the induced electric field is supported by theoretical analysis of the Cabrera–Mott effect for oxide coated nanoparticles.[21] Oxidation initiation by rapid diffusion of aluminum ions to the nanoparticle surface is in agreement with published experimental efforts that have observed the formation of hollow aluminum oxide nanoparticles.[9,10] Diffusion of oxygen ions into the shell has also been considered but does not contribute appreciably when compared to the flux of aluminum to the nanoparticle surface.

ACKNOWLEDGMENTS

The authors would like to acknowledge the support received by the U.S. Army Research Laboratory DoD Supercomputing Resource Center (DSRC) at the Aberdeen Proving Ground, MD. Additional support was provided by the U.S. Army Research Office (ARO).

[1] X. Phung, J. Groza, E. A. Stach, L. N. Williams, and S. B. Ritchey, Mater. Sci. Eng., A **359**, 261 (2003).
[2] J. H. Sinfelt, *Bimetallic Catalysis: Discoveries, Concepts and Applications* (Wiley, New York, 1983).
[3] J. Uppenbrink and J. David, J. Chem. Phys. **96**, 8520 (1992).
[4] A. Rai, D. Lee, K. Park, and M. R. Zachariah, J. Phys. Chem. B **108**, 14793 (2004).
[5] M. A. Trunov, M. Shoenitz, and E. L. Dreizin, Combust. Theory Modell. **10**, 603 (2006).
[6] V. I. Levitas, B. W. Asay, S. F. Son, and M. Pantoya, Appl. Phys. Lett. **89**, 071909 (2006).
[7] V. I. Levitas, B. W. Asay, S. F. Son, and M. Pantoya, J. Appl. Phys. **101**, 083524 (2007).
[8] P. Puri and V. Yang, in Proceedings of the 46th AIAA Aerospace Sciences Meeting and Exhibit, Paper No. AIAA–2008–0938, Reno, NV, 7–10 January 2008 (Curran Associates, Inc., NY, 2008).
[9] A. Rai, K. Park, L. Zhou, and M. R. Zachariah, Combust. Theory Modell. **10**, 843 (2006).
[10] R. Nakamura, D. Tokozakura, H. Nakajima, J.-G. Lee, and H. Mori, J. Appl. Phys. **101**, 074303 (2007).
[11] N. Cabrera and N. F. Mott, Rep. Prog. Phys. **12**, 163 (1949).
[12] A. T. Fromhold, Jr. and E. L. Cook, Phys. Rev. **163**, 650 (1967).
[13] C. Wagner, Z. Phys. Chem. **B21**, 25 (1933).
[14] L. P. H. Jeurgens, W. G. Sloof, F. D. Tichelaar, and E. J. Mittemeijer, J. Appl. Phys. **92**, 1649 (2002).
[15] A. C. T. van Duin, S. Dasgupta, F. Lorant, and W. A. Goddard III, J. Phys. Chem. A **105**, 9396 (2001).
[16] F. H. Streitz and J. W. Mintmire, Phys. Rev. B **50**, 11996 (1994).
[17] Q. Zhang, T. Çağın, A. van Duin, W. A. Goddard III, Y. Qi, and L. G. Hector, Jr., Phys. Rev. B **69**, 045423 (2004).
[18] N. Pradeep, D. I. Kim, J. Grobelny, T. Hawa, B. J. Henz, and M. R. Zachariah, Appl. Phys. Lett. **91**, 203114 (2007).
[19] S. Ogata, H. Iyetomi, K. Tsuruta, F. Shimojo, A. Nakano, R. K. Kalia, and P. Vashishta, J. Appl. Phys. **88**, 6011 (2000).
[20] P. P. Mitra, P. N. Sen, L. M. Schwartz, and P. Le Doussal, Phys. Rev. Lett. **68**, 3555 (1992).
[21] V. P. Zhdanov and B. Kasemo, Chem. Phys. Lett. **452**, 285 (2008).
[22] C. G. Zoski, *Handbook of Electrochemistry* (Elsevier, New York, 2007).
[23] J. Dalla Torre, J.-L. Bocquet, Y. Limoge, J.-P. Crocombette, E. Adam, G. Martin, T. Baron, P. Rivallin, and P. Mur, J. Appl. Phys. **92**, 1084 (2002).
[24] V. Zhukov, I. Popova, and J. T. Yates, Surf. Sci. **441**, 251 (1999).